fractal and fractional

MDPI

Article

A Look-Up Table Based Fractional Order Composite Controller Synthesis Method for the PMSM Speed Servo System

Weijia Zheng [1,*], Runquan Huang [1], Ying Luo [2], YangQuan Chen [3], Xiaohong Wang [4] and Yong Chen [1]

[1] School of Mechatronic Engineering and Automation, Foshan University, 33 Guangyun Road, Foshan 528225, China; 2112052019@stu.fosu.edu.cn (R.H.); cheny@fosu.edu.cn (Y.C.)
[2] Department of Mechanical Science and Engineering, Huazhong University of Science and Technology, 1037 Luoyu Road, Wuhan 430074, China; ying.luo@hust.edu.cn
[3] School of Engineering, University of California Merced, 5200 North Lake Road, Merced, CA 95340, USA; ychen53@ucmerced.edu
[4] School of Automation Science and Engineering, South China University of Technology, 381 Wushan Road, Guangzhou 510641, China; xhwang@scut.edu.cn
* Correspondence: wjzheng@fosu.edu.cn

Abstract: Considering the performance requirements in actual applications, a look-up table based fractional order composite control scheme for the permanent magnet synchronous motor speed servo system is proposed. Firstly, an extended state observer based compensation scheme was adopted to suppress the motor parametric uncertainties and convert the speed servo plant into a double-integrator model. Then, a fractional order proportional-derivative (PD^{μ}) controller was adopted as the speed controller to provide the optimal step response performance for the servo system. A universal look-up table was established to estimate the derivative order of the PD^{μ} controller, according to the optimal samples collected by an improved differential evolution algorithm. With the look-up table, the optimal PD^{μ} controller can be tuned analytically. Simulation and experimental results show that the servo system using the composite control scheme can achieve optimal tracking performance and has robustness to the motor parametric uncertainties and disturbance torques.

Keywords: permanent magnet synchronous motor (PMSM); extended state observer (ESO); PD^{μ} controller; look-up table; differential evolution (DE)

Citation: Zheng, W.; Huang, R.; Luo, Y.; Chen, Y.; Wang, X.; Chen, Y. A Look-Up Table Based Fractional Order Composite Controller Synthesis Method for the PMSM Speed Servo System. *Fractal Fract.* **2022**, *6*, 47. https://doi.org/10.3390/fractalfract6010047

Academic Editor: Norbert Herencsar

Received: 17 December 2021
Accepted: 11 January 2022
Published: 15 January 2022

1. Introduction

With high power density and efficiency, the permanent magnet synchronous motor (PMSM) has been widely used in modern industrial applications, e.g., numerical control machines and industrial robots. It is widely known that the proportional–integral–derivative (PID) control approach is the most widely used in the industrial field, because of its simple implementation and clear physical meaning in control engineering [1]. However, in actual applications, the PMSM servo system is unavoidably faced with various uncertainties and disturbances [2,3]. The traditional feedback control method may find it difficult to provide good tracking performance and disturbance rejection performance simultaneously [4]. A composite control strategy may be an efficient way to improve the performance. By introducing a feedforward compensation, the composite control strategy allows the separate regulation of the tracking performance and the disturbance rejection performance. The commonly used composite control methods include the disturbance observer-based control (DOBC) method [5] and the active disturbance rejection control (ADRC) method [6]. By applying the ADRC method, the uncertainties and disturbances of the system are estimated by an extended state observer (ESO) and compensated by the feedforward compensation [7]. Therefore, the composite control method provides the possibility to ensure the good tracking performance and disturbance rejection performance simultaneously.

In the last few decades, fractional calculus has been continuously developed in system modeling and control fields [8–10]. Fractional differential systems have been widely

studied and applied to describe various real systems and processes [11–14]. Recently, various strategies based on fractional calculus have been developed and applied to different areas, such as feedback control, disturbance estimation and signal processing [15–17]. In addition, fractional order controllers have been found to obtain more control options and flexibility than integer order controllers. The fractional order proportional–integral–derivative ($PI^{\lambda}D^{\mu}$) controller is derived from the conventional PID controller by extending the integral and derivative orders from 1 to real numbers [18,19]. It is reported that a $PI^{\lambda}D^{\mu}$ controller can provide more flexibility and better control performance than a PID controller [20,21]. Meanwhile, with two additional tunable parameters, more sophisticated strategies are required when designing a $PI^{\lambda}D^{\mu}$ controller [22].

Generally, the design methods of a $PI^{\lambda}D^{\mu}$ controller include the analytic methods and the optimization methods. The "flat-phase" design method is a typical analytic design method [23]. By introducing a tuning rule called the flat-phase specification, this method configures the control system's phase characteristic to obtain a zero slope at the gain crossover frequency. In contrast, the optimization design method tunes the controller by optimizing an objective function, which is often introduced to characterize the specific demands on system performance, such as the dynamic performance, stability and robustness [8,15]. In addition, the controller's parameters are often optimized within the feasible regions constructed by different constraints characterizing practical restrictions on the control systems [24]. Thus, the optimized $PI^{\lambda}D^{\mu}$ controller can achieve the optimal dynamic performance under different constraints. However, in real applications, these methods may need time and high-performance control chips to finish optimization.

In this paper, taking advantage of fractional order controllers and the composite control strategy, a fractional order composite control method is proposed to improve both the robustness and the dynamic performance of a class of PMSM servo systems. Firstly, ESO-based feedforward compensation was adopted to compensate the lumped disturbance and convert the PMSM speed servo plant into a general double-integrator model. Secondly, a fractional order PD^{μ} controller was adopted as the feedback controller to provide the optimal step response performance. To simplify the tuning process of the PD^{μ} controller, a universal look-up table was established to estimate the derivative order of the PD^{μ} controller, according to the optimal samples collected by an improved differential evolution (DE) algorithm [25]. With the estimated derivative order, the PD^{μ} controller can be tuned analytically based on the design specifications.

The composite control method was applied to the PMSM speed servo system. Simulations and experiments were implemented to test the robustness, the step response and load disturbance response performances, respectively. In addition, the control performance of the proposed scheme is compared with those of some commonly used approaches. The advantages of the composite control scheme are demonstrated by simulation and experimental results.

The contributions of this paper mainly include:

1. A composite control scheme is presented, providing the optimal dynamic performance and sufficient robustness for the PMSM speed servo system;
2. A look-up table based synthesis method is proposed to simplify the tuning of the optimal PD^{μ} controller, creating a wide potential application scope for the proposed method.

The content of this paper is arranged as follows: the PMSM speed control problem is described in Section 2; the fractional order composite controller synthesis method is discussed in Section 3; the simulation and experimental studies of the composite control scheme are presented in Section 4; the conclusions are discussed in Section 5.

2. PMSM Speed Control Problem

The commonly used rotor synchronous rotating coordinates (*d*-*q* coordinates) are adopted as the reference coordinates, where the *d*-axis is synchronized with the rotor flux

vector and the q-axis is perpendicular to the d-axis. Thus, the model of a three-phase rotating PMSM can be described by the following equations [4],

$$\dot{i}_d = \frac{1}{L_d}(u_d - Ri_d + n_p\omega L_q i_q), \tag{1}$$

$$\dot{i}_q = \frac{1}{L_q}(u_q - Ri_q - n_p\omega L_d i_d - n_p\omega\psi_f), \tag{2}$$

$$\dot{\omega} = \frac{1}{J}(T_e - T_f - T_L), \tag{3}$$

$$T_e = \frac{3}{2}n_p[\psi_f i_q + (L_d - L_q)i_d i_q], \tag{4}$$

where

i_d, i_q: d- and q-axis stator currents, respectively;
u_d, u_q: d and q-axis stator voltages, respectively;
L_d, L_q: d and q-axis stator inductances, respectively;
R: stator resistance;
n_p: pole pairs number;
ω: motor angular velocity;
ψ_f: magnetic flux linkage;
J: motor rotating inertia;
T_f, T_L: friction and load torques, respectively.

When adopting the common field-oriented vector control scheme, with the reference current ${i_d}^*$ set to be 0, the d-axis stator current i_d will be close to 0 under the control of the current controller. Thus, (2) can be simplified as

$$\dot{i}_q = \frac{1}{L_q}(u_q - Ri_q - n_p\omega\psi_f). \tag{5}$$

Since the variation of i_q is much faster than that of ω, the back electromotive force (EMF) $n_p\omega\psi_f$ can be approximated as a constant disturbance when designing the q-axis current controller [26].

By adopting a PI controller as the q-axis current controller,

$$u_q(t) = K_s e(t) + \frac{K_s R}{L_q}\int_0^t e(\tau)d\tau, \tag{6}$$

where $e = {i_q}^* - i_q$, ${i_q}^*$ is the q-axis reference current. Thus, the PMSM speed servo plant can be approximated as the following:

$$\dot{i}_q = -\frac{K_s}{L_q}i_q + \frac{K_s}{L_q}{i_q}^*, \tag{7}$$

$$\dot{\omega} = \frac{C_m}{J}i_q - \frac{T_d}{J}, \tag{8}$$

where C_m represents the torque coefficient: $C_m = 3n_p\psi_f/2$; T_d represents the total disturbance torque: $T_d = T_f + T_L$. In this paper, adopting a common simplified assumption in motion control research, T_d is assumed to be a slowly-varying disturbance, i.e., $\dot{T}_d \approx 0$ [27,28]. Assume that the feedback controller of the PMSM servo system is $C(s)$. According to (7) and (8), the transfer function from T_d to ω can be represented as

$$G_{T_d\to\omega}(s) = \frac{L_q s/K_s + 1}{Js(L_q s/K_s + 1) + C(s)}. \tag{9}$$

According to the internal model principle, the feedback controller should contain an integrator to completely eliminate the tracking error of the motor velocity caused by the slowly-varying disturbance. However, in some cases, the integrator in the feedback controller may lead to large overshooting and oscillations. Therefore, it may be difficult to design a feedback controller to achieve good step response performance and disturbance rejection performance simultaneously. This paper mainly addresses a composite control method to make the PMSM servo system achieve optimal step response performance and sufficient rejection of the slowly-varying disturbance torque.

3. Fractional Order Composite Control Strategy

3.1. Eso-Based Composite Control Scheme

The q-axis current loop represented by (7) is an ideal model. An actual PMSM servo system may have unmodeled dynamics and parametric uncertainties. Thus, (7) should be modified as

$$\dot{i}_q = -\frac{K_s}{L_q} i_q + \frac{K_s}{L_q} {i_q}^* + \varepsilon = h + b_0 {i_q}^*, \tag{10}$$

where $b_0 = K_s/L_q$; ε represents the effect of the unmodeled dynamics and uncertainties; $h = -b_0 i_q + \varepsilon$, which is regarded as the lumped disturbance. By defining $x_1 = i_q$ and introducing an extended state $x_2 = h$, (10) can be represented as

$$\begin{aligned} \dot{x}_1 &= x_2 + b_0 {i_q}^*, \\ \dot{x}_2 &= \dot{h}. \end{aligned} \tag{11}$$

According to the ADRC strategy, an ESO is applied to estimate the state and lumped disturbance of the control system. Thus, a commonly used linear ESO is derived for system (11) [29],

$$\begin{aligned} \dot{z}_1 &= z_2 + b_0 {i_q}^* + \beta_1 (x_1 - z_1), \\ \dot{z}_2 &= \beta_2 (x_1 - z_1), \end{aligned} \tag{12}$$

where z_1 and z_2 are the estimates of i_q and h, respectively; and β_1 and β_2 are the observer gains. When adopting a bandwidth design method, the observer gains are set as $\beta_1 = 2\omega_0$, $\beta_2 = {\omega_0}^2$, where ω_0 represents the bandwidth of the ESO.

According to the estimated lumped disturbance, the control law is designed as

$${i_q}^* = u_0 - \frac{z_2}{b_0}. \tag{13}$$

where u_0 represents the output of the speed controller. Therefore, the q-axis current loop with ESO-based compensation can be represented as Figure 1.

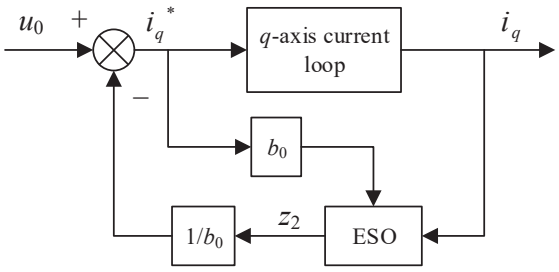

Figure 1. ESO-based q-axis current loop.

Assume that the lumped uncertainties satisfy $\lim_{t\to\infty} \dot{h}(t) = 0$. If the ESO is suitably designed, the estimation error of the ESO, $h - z_2$ will converge to zero. Then, by combin-

ing (10) and (13), the q-axis current loop with the ESO-based feedforward compensation can be approximated as an integrator:

$$\dot{i}_q = b_0 u_0 + (h - z_2) \approx b_0 u_0. \tag{14}$$

Combining (14) and (8), under the slowly-varying disturbance torque, the PMSM speed servo plant can be reduced to a double-integrator model:

$$\ddot{\omega} \approx \frac{C_m b_0}{J} u_0, \tag{15}$$

Thus, with the ESO-based feedforward compensation, the tracking error of the motor velocity caused by the slowly-varying disturbance torque can be completely eliminated.

A PD$^\mu$ controller is adopted as the speed controller. The PD$^\mu$ controller can be represented as

$$C(s) = K_p(1 + K_d s^\mu), \tag{16}$$

where K_p and K_d are the proportional and derivative gains, respectively; and D^μ represents the differential operator with real-number order μ, $\mu \in (0, 2)$. Taking the deviation between the reference and actual angular velocity as the input, the output of the speed controller can be represented as

$$u_0 = K_p(1 + K_d D^\mu)(\omega_r - \omega), \tag{17}$$

where ω_r is the reference velocity.

By combining (15) and (17), the transfer function of the closed-loop system with the PD$^\mu$ controller and the double-integrator plant can be obtained:

$$G_c(s) = \frac{cb_0 K_p(1 + K_d s^\mu)}{s^2 + cb_0 K_p K_d s^\mu + cb_0 K_p}, \tag{18}$$

where c represents the term C_m/J.

3.2. Stability

A system is said to be bounded-input bounded-output (BIBO) stable if every bounded input excites a bounded output. A linear time-invariant (LTI) system is BIBO-stable if and only if all poles of its transfer function are in the left half of the complex plane [30]. Let $e_1 = x_1 - z_1$ and $e_2 = x_2 - z_2$. According to (11) and (12), the estimation error equation can be obtained:

$$\begin{bmatrix} \dot{e}_1 \\ \dot{e}_2 \end{bmatrix} = \begin{bmatrix} -\beta_1 & 1 \\ -\beta_2 & 0 \end{bmatrix} \begin{bmatrix} e_1 \\ e_2 \end{bmatrix} + \begin{bmatrix} 0 \\ 1 \end{bmatrix} \dot{h}. \tag{19}$$

Thus, the characteristic polynomial of the estimation error equation can be represented as

$$\lambda(s) = s^2 + \beta_1 s + \beta_2. \tag{20}$$

Therefore, the linear ESO described in (12) is BIBO-stable if all the roots of the characteristic polynomial have negative real parts [29].

Theorem 1. *The composite control design according to (12), (13) and (17) obtains a BIBO-stable control system if the ESO in (12) and the control law (17) for the double-integrator model are stable, and T_d and $\dot{h}$ are bounded.*

Proof. By combining (8), (11), (12), (13) and (17), the composite control system can be represented by the following state equations.

$$\begin{aligned}
\dot{\omega} &= cx_1 + d,\\
\dot{x}_1 &= x_2 - z_2 + b_0K_p(1 + K_dD^\mu)(\omega_r - \omega),\\
\dot{x}_2 &= \dot{h},\\
\dot{z}_1 &= \beta_1(x_1 - z_1) + b_0K_p(1 + K_dD^\mu)(\omega_r - \omega),\\
\dot{z}_2 &= \beta_2(x_1 - z_1).
\end{aligned} \tag{21}$$

where $d = -T_d/J$. Under zero initial conditions, the following equations can be derived by using the Laplace transform.

$$\begin{aligned}
s\omega(s) &= cx_1(s) + d(s),\\
sx_1(s) &= h(s) - \frac{\beta_2}{s}(x_1(s) - z_1(s)) + b_0K_p(1 + K_dD^\mu)(\omega_r(s) - \omega(s)),\\
sz_1(s) &= \beta_1(x_1(s) - z_1(s)) + b_0K_p(1 + K_dD^\mu)(\omega_r(s) - \omega(s)).
\end{aligned} \tag{22}$$

Then the angular velocity $\omega(s)$ can be derived by solving (22):

$$\begin{aligned}
\omega(s) = &\frac{cb_0K_p\omega_r(s)}{s^2 + cb_0K_pK_ds^\mu + cb_0K_p}\\
&+ \frac{c(s^2 + \beta_1 s)h(s)}{(s^2 + \beta_1 s + \beta_2)(s^2 + cb_0K_pK_ds^\mu + cb_0K_p)}\\
&+ \frac{sd(s)}{s^2 + cb_0K_pK_ds^\mu + cb_0K_p}.
\end{aligned} \tag{23}$$

It can be observed that the eigenvalues of the closed-loop system are the roots of the characteristic polynomials of the ESO's estimation error (see (20)) and the closed-loop system with the PD$^\mu$ controller and the double-integrator model (see (18)). Since ω_r, T_d and $\dot{h}$ are bounded, the composite control system is BIBO-stable if its eigenvalues have negative real parts, i.e., both the ESO and the system with the PD$^\mu$ controller and the double-integrator model are stable. □

The PMSM speed servo system with the ESO-based compensation can be represented as Figure 2, where n^* and n represent the reference and actual motor speed, respectively; $n = 60\omega/(2\pi)$; and $C_v(s)$ represents the speed controller. Thus, the PMSM speed servo model (from u_0 to n) can be approximated in a double-integrator model:

$$P(s) = \frac{K}{s^2}, \tag{24}$$

where $K = 60b_0C_m/(2\pi J)$.

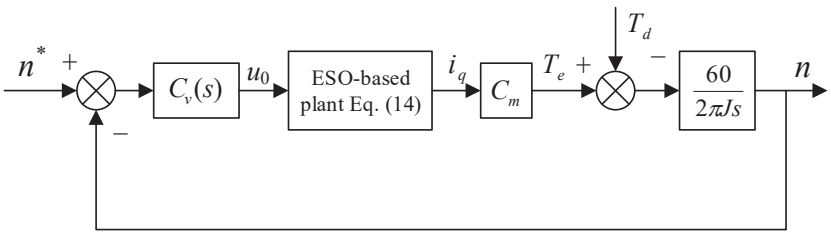

Figure 2. The PMSM speed servo system with the ESO-based compensation.

Remark 1. *By introducing the ESO-based feedforward compensation, the PMSM speed servo plants with different parameters can be converted into the double-integrator models with different gains. Under slowly-varying disturbances, the feedback controller can ensure zero speed deviation*

without using an integrator. In addition, the model's gain can be directly compensated by the gain of the feedback controller. Therefore, the ESO-based control scheme creates the possibility to design the universal feedback controllers for different PMSM speed servo systems.

3.3. Optimal PD$^{\mu}$ *Controller Design*

Optimal control is to select a permissible control law that allows the control system to achieve the optimal performance, which is often quantized by a loss function [31]. In this paper, the PD$^{\mu}$ controller is designed to ensure the optimal step response performance of the servo system, under the given design specifications (ω_c, φ_m). Suppose that ω_c and φ_m are given. Two equations can be derived:

$$|C(j\omega_c)P(j\omega_c)| = 1, \tag{25}$$

$$\text{Arg}[C(j\omega_c)] + \text{Arg}[P(j\omega_c)] = \varphi_m - \pi, \tag{26}$$

where $\text{Arg}[P(j\omega)]$ and $\text{Arg}[C(j\omega)]$ represent the phase of the plant model and the PD$^{\mu}$ controller, respectively. Thus, if the derivative order μ is determined, K_p and K_d can be calculated according to (25) and (26).

The performance of the PD$^{\mu}$ controller is quantified by the following loss function.

$$J = \kappa_1 \int_0^{\infty} t|\epsilon(t)|dt + \kappa_2 \int_0^{\infty} |u_0(t)|dt, \tag{27}$$

where $\epsilon(t) = n^*(t) - n(t)$; $u_0(t)$ is the controller's output. Thus, the first term represents the integrated time absolute error (ITAE) of the motor speed, and the second term represents the energy consumption of the control signal. κ_1 and κ_2 are the weights used to balance the requirements of the tracking performance and energy consumption [32].

An improved DE algorithm was implemented in *Matlab* to determine the derivative order μ. At first, the population is initialized by randomly selecting N values of μ to be the individuals. Then, the PD$^{\mu}$ controller corresponding to each individual (μ) is obtained by solving (25) and (26), according to the design specifications (ω_c, φ_m).

Secondly, when the population is generated, several individuals are randomly selected as the target individuals according to a given mutation rate. Taking advantage of the adaptive parameter strategies [33], an adaptive mutation rate is proposed to enhance the efficiency of the algorithm. The mutation rate $P_{m,i}$ in the mth iteration for the ith individual is defined as

$$P_{m,i} = P_0 \cdot 2^{\gamma}, \gamma = e^{\frac{1-m}{1-m+m_s} \cdot \frac{F_i - F_l + \delta_l}{F_u - F_l + \delta_l}}, \tag{28}$$

where P_0 is the initial mutation rate; m_s is the upper limit of the iteration count; F_i is the fitness of the ith individual; F_u and F_l are the largest and smallest fitness values of the current population, respectively; and δ_l is a factor used to keep $F_u - F_l + \delta_l$ larger than zero. The term $(1-m)/(1-m+m_s)$ is used to tune the basic mutation rate in each iteration: at the beginning of the iteration, it is close to zero and then the basic mutation rate is close to $2P_0$, suitable for keeping the individual diversity and avoiding the over-expansion of the local optimal individuals. Late in the iteration process, it decreases to close to $1-m$ and the basic mutation rate is close to P_0, suitable for protecting the potential global optimal individual from being mutated. In addition, the term $(F_i - F_l + \delta_l)/(F_u - F_l + \delta_l)$ is used to tune the mutation rate of each individual: an individual with less fitness has a larger mutation rate to explore the searching space, whereas one with more fitness has a smaller mutation rate.

Once a target individual is selected, a mutated individual will be generated by adding a difference vector to the target individual:

$$V_i = X_i + k(X_j - X_k), \tag{29}$$

where V_i represents the mutated individual, X_i represents the target individual, X_j and X_k are two randomly selected individuals and k is a scaler coefficient. In addition, the PD$^\mu$ controllers corresponding to the mutated individuals are also obtained.

Thirdly, the step response simulations are implemented on the *Simulink* platform, which was constructed according to the closed-loop system shown in Figure 2. Customized constraints can be introduced into the simulation modules. In this study, the output saturation was introduced according to the amplitude limitation of the actuator. The PD$^\mu$ controller corresponding to each individual was used as the speed controller. The fitness of each individual is defined as the reciprocal of the loss function of the control system, i.e., $F_i = 1/J_i$.

Finally, a comparison is performed between the mutated and target individuals: the one with greater fitness will be selected in the population, while the other one will be abandoned. The termination condition of the optimization is determined as follows: if the variation of the population's average fitness in the latest 10 iterations is smaller than a threshold δ, or the iteration count reaches the upper limit, the optimization will be ended.

According to (24) and (26), the parameters of the PMSM and q-axis current controller have no effect on the derivative order of the optimal PD$^\mu$ controller. Therefore, a universal look-up table of the derivative order with respect to different design specifications can be established to simplify the controller design process. The look-up table is established within the ranges of ω_c and φ_m. The range of ω_c was set as 30 to 80 rad/s. In addition, the range of φ_m was set as 30° to 60°, in accordance with the general selection of the phase margin in engineering applications [26,34]. According to the ranges of ω_c and φ_m, several values were selected uniformly, obtaining the sequences of ω_c (30 rad/s, 35 rad/s, …, 80 rad/s) and φ_m (30°, 35°, …, 60°). Therefore, the design specification pairs (ω_c, φ_m) could be constructed by combining the selected values of ω_c and φ_m in sequence. Taking the double-integrator model (24) as the controlled plant, the PD$^\mu$ controller corresponding to each design specification pair was obtained by applying the DE algorithm. The parameters of the DE algorithm were selected as follows: $N = 20$, $m_s = 100$, $P_0 = 0.1$, $k = 0.5$, $\delta = 0.0001$. The look-up table of the derivative order μ for different design specifications is presented in Table 1.

Table 1. Look-up table of the derivative order μ for different design specifications.

φ_m (°)	ω_c (rad/s)										
	30	**35**	**40**	**45**	**50**	**55**	**60**	**65**	**70**	**75**	**80**
30	0.765	0.781	0.795	0.808	0.820	0.831	0.842	0.852	0.861	0.869	0.878
35	0.806	0.823	0.836	0.848	0.859	0.869	0.879	0.887	0.893	0.900	0.907
40	0.845	0.861	0.872	0.883	0.891	0.899	0.907	0.914	0.920	0.927	0.933
45	0.881	0.893	0.903	0.911	0.919	0.926	0.931	0.935	0.939	0.942	0.946
50	0.911	0.922	0.930	0.937	0.941	0.944	0.948	0.950	0.954	0.956	0.959
55	0.939	0.946	0.952	0.956	0.959	0.962	0.964	0.967	0.968	0.970	0.972
60	0.962	0.968	0.972	0.975	0.977	0.978	0.980	0.981	0.982	0.983	0.984

If the design specifications are located within the grids of the look-up table, the derivative order can be estimated applying a commonly used bilinear interpolation method [35]. As shown in Figure 3, the derivative order of the target point (ω_c, φ_m) is estimated based on the four nearest rectangular points surrounding the target point, using the following formula.

$$\mu(\omega_c, \varphi_m) = w_1\mu_1 + w_2\mu_2 + w_3\mu_3 + w_4\mu_4, \tag{30}$$

where

$$
\begin{aligned}
w_1 &= \frac{(\omega_{c2}-\omega_c)(\varphi_{m2}-\varphi_m)}{(\omega_{c2}-\omega_{c1})(\varphi_{m2}-\varphi_{m1})},\\
w_2 &= \frac{(\omega_c-\omega_{c1})(\varphi_{m2}-\varphi_m)}{(\omega_{c2}-\omega_{c1})(\varphi_{m2}-\varphi_{m1})},\\
w_3 &= \frac{(\omega_{c2}-\omega_c)(\varphi_m-\varphi_{m1})}{(\omega_{c2}-\omega_{c1})(\varphi_{m2}-\varphi_{m1})},\\
w_4 &= \frac{(\omega_c-\omega_{c1})(\varphi_m-\varphi_{m1})}{(\omega_{c2}-\omega_{c1})(\varphi_{m2}-\varphi_{m1})}.
\end{aligned} \tag{31}
$$

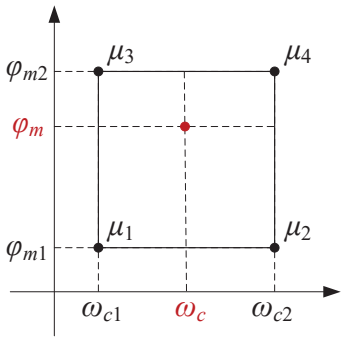

Figure 3. Estimation of the derivative order based on the four nearest rectangular points.

The effectiveness of the look-up table was verified by the estimation error tests. Several PD$^\mu$ controllers were designed as the test samples using the DE algorithm, based on the design specifications constructed by the elements in the sequences of ω_c and φ_m: (35 rad/s, 45rad/s, ..., 75rad/s) and (35°, 45°, 55°). An estimation error was defined as (32) to quantify the deviation between the derivative order obtained using the optimization method and that estimated by the look-up table:

$$\Delta(\%) = \frac{|\mu_o - \mu_e|}{\mu_o} \times 100\%, \tag{32}$$

where μ_o and μ_e represent the derivative orders obtained using the DE algorithm and the look-up table, respectively. The estimation errors corresponding to different design specifications are listed in Table 2. It can be observed that all the estimation errors are smaller than 0.1%. Thus, the derivative orders estimated by the look-up table can be regarded as the optimal values.

Table 2. Estimation error of the derivative orders.

φ_m (°)	ω_c (rad/s)				
	35	**45**	**55**	**65**	**75**
35	0.059%	0.030%	0.017%	0.071%	0.008%
45	0.014%	0.005%	0.009%	0.054%	0.006%
55	0.003%	0.002%	0.009%	0.004%	0.021%

Remark 2. *In actual applications, a PMSM speed servo model can be converted into a double-integrator model by the ESO-based scheme. Then, the derivative order of the* PD$^\mu$ *controller can be estimated by the universal look-up table. The remaining parameters of the controller can be calculated according to (25) and (26). In this way, the* PD$^\mu$ *controller of the servo system can be designed without optimization, which may be suitable for actual applications.*

4. Application to the PMSM Speed Control Problem

The composite control scheme was applied to the PMSM speed control problem. The robustness, step response performance and disturbance rejection performance of the control system using the proposed controller were tested. In simulations and experiments, the PD$^{\mu}$ controller was approximated by an impulse response invariant discretization method [36]. While applying this method, the impulse response of the fractional operator was calculated according to the Riemann–Liouville definition of fractional calculus [37], and then fitted by a rational discrete transfer function.

4.1. Simulation Studies

Simulations were implemented on the *Simulink* platform to verify the composite control system's robustness to the parametric uncertainties. The parameters of the PMSM module were set as: $R = 0.5\ \Omega$, $L_q = 5$ mH, $J = 0.03$ kg·m^2, $C_m = 0.6$ N·m/A. Then the q-axis current controller was obtained.

$$C_{is}(s) = 1.289\left(1 + \frac{100}{s}\right). \tag{33}$$

Therefore, $b_0 = 257.7$. A common rule of thumb is to choose the bandwidth of the ESO with $\omega_0 = 3\sim5\omega_c$ [29]. The design specifications were $\omega_c = 70$ rad/s, $\varphi_m = 60^\circ$. Therefore, ω_0 was selected to be 300 rad/s. According to the parameters of the PMSM, the double-integrator model of the PMSM speed servo plant was $P(s) = 60b_0C_m/(2\pi Js^2) = 49,217.1/s^2$.

According to the design specifications, the derivative order of the PD$^{\mu}$ controller should be estimated by the look-up table: $\mu = 0.982$. Therefore, the PD$^{\mu}$ controller was obtained by solving (25) and (26):

$$C_v(s) = 0.047(1 + 0.0281s^{0.982}). \tag{34}$$

The stator resistance R has been found to vary with the temperature, which has an impact on the control performance [2]. To verify the robustness of the composite control system to the stator resistance uncertainties, PMSM modules with different resistances, i.e., 0.1 Ω, 0.5 Ω and 1 Ω, were used for step response simulations. The speed response curves are plotted in Figure 4. It can be observed that the systems with stator resistance uncertainties achieved nearly the same speed response as the nominal system.

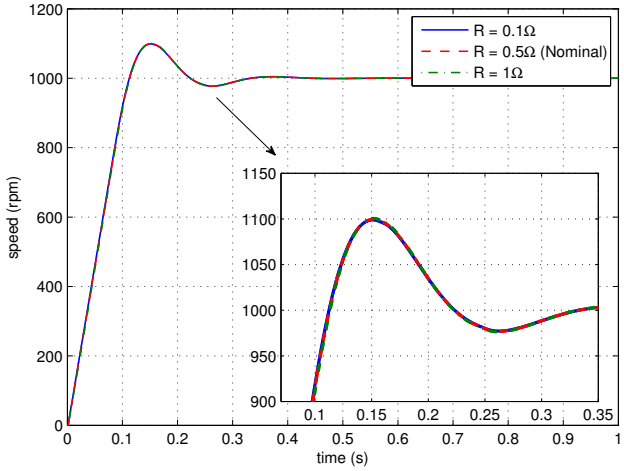

Figure 4. Tests of robustness to stator resistance uncertainties.

The stator inductance L_q of the PMSM has been found to be the function of the current magnitude and phase angle [2]. Since the compensation gain b_0 is determined by the nominal stator inductance L_q, the variations of L_q may degrade the performance of the servo system. To verify the robustness of the composite control system to the stator

inductance uncertainties, PMSM modules with different inductances, i.e., 2, 5 and 10 mH, were used for step response simulations. The speed response curves are plotted in Figure 5. It can be observed that the systems with stator inductance uncertainties also achieved nearly the same speed response as the nominal system.

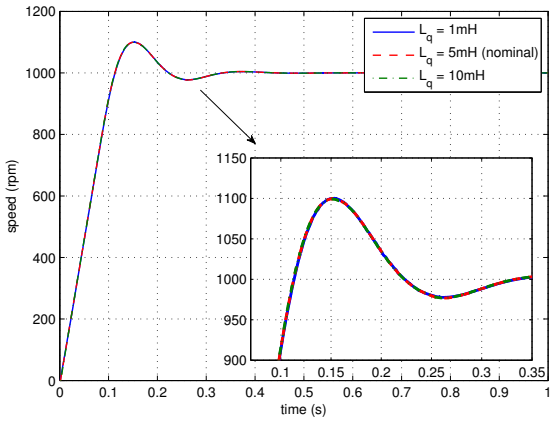

Figure 5. Tests of robustness to stator inductance uncertainties.

According to the simulation results, under the proposed composite control scheme, the control system obtains sufficient robustness to the motor parametric uncertainties.

4.2. Experimental Studies

The PMSM speed control experimental platform is shown in Figure 6. The PMSM was driven by a DSP-based servo driver. A DC generator and a resistance box were used to provide the resistive load of the servo system. The parameters of the PMSM were R = 0.5 Ω, L_q = 3.75 mH, C_m = 0.66 N·m/A, and J = 0.0336 kg·m^2.

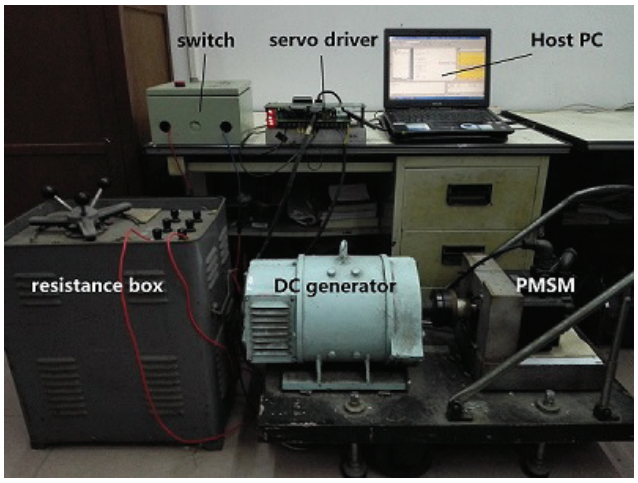

Figure 6. PMSM speed control experimental platform.

4.2.1. Comparison with the Composite Control Method Using the PD Controller

According to the composite control scheme, the PD$^{\mu}$ controller was used to make the servo system achieve the optimal step response performance. To demonstrate the advantage of using the PD$^{\mu}$ controller, a performance comparison was performed between the FOPD-ESO controller and the integer order PD controller with the ESO (denoted as IOPD-ESO).

According to the parameters of the PMSM, the q-axis current controller was designed:

$$C_{ie}(s) = 0.966\left(1 + \frac{133.33}{s}\right). \tag{35}$$

Thus, $b_0 = 257.7$. The design specifications were $\omega_c = 70$ rad/s and $\varphi_m = 60°$. Therefore, ω_0 was selected to be 300 rad/s. The double-integrator model of the PMSM speed servo plant was $P(s) = 48{,}338.5/s^2$. The derivative order μ of the PD$^\mu$ controller was 0.982. Therefore, the PD$^\mu$ controller was obtained:

$$C_1(s) = 0.048(1 + 0.0281s^{0.982}). \tag{36}$$

According to the same design specifications, an integer order PD controller was obtained by solving (25) and (26) with $\mu = 1$.

$$C_2(s) = 0.051(1 + 0.0247s). \tag{37}$$

Step responses were implemented on the experimental platform. The motor speed and q-axis current of the systems using the IOPD-ESO and FOPD-ESO are plotted in Figure 7. In addition, the quantitative performance comparisons are presented in Table 3. It can be observed that the FOPD-ESO controller provided the better step response performance.

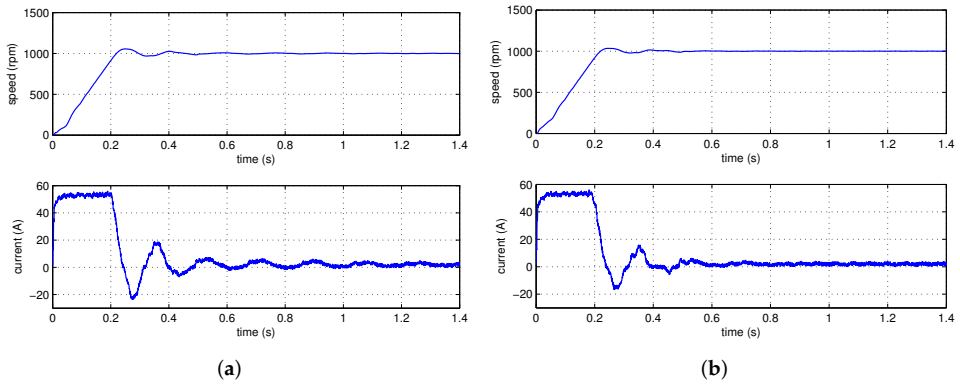

Figure 7. Step response comparisons. (**a**) IOPD-ESO. (**b**) FOPD-ESO.

Table 3. Step response performances of IOPD-ESO and FOPD-ESO.

Index	IOPD-ESO	FOPD-ESO
Settling time (s)	0.266	0.207
Overshoot (%)	5.51	3.41

Load increase responses were also tested on the experimental platform. The partial enlarged curves of the motor speed and q-axis current of the systems using the IOPD-ESO and FOPD-ESO are plotted in Figure 8. In addition, the quantitative performance comparisons are presented in Table 4. It can be observed that the control system using the FOPD-ESO controller had a shorter recovery time.

Table 4. Load disturbance response performances of IOPD-ESO and FOPD-ESO.

Index	IOPD-ESO	FOPD-ESO
Dynamic speed drop (%)	2.59	2.30
Recovery time (s)	0.122	0.052

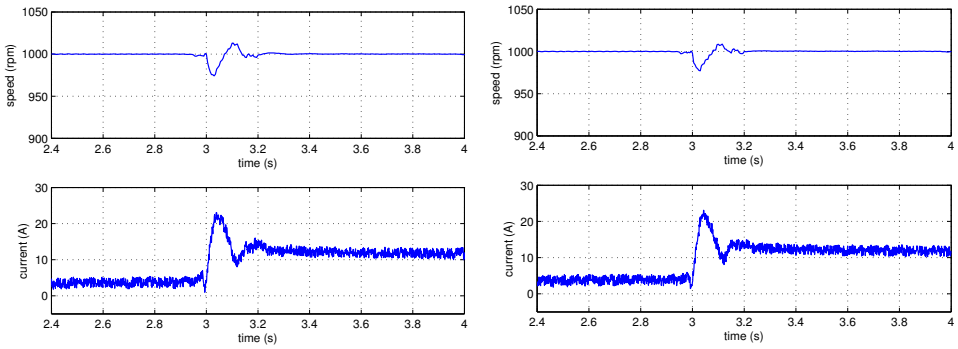

(**a**) (**b**)

Figure 8. Load disturbance response comparisons. (**a**) IOPD-ESO. (**b**) FOPD-ESO.

4.2.2. Comparisons with Some Fractional Order Controllers

Secondly, the proposed control scheme was compared with some commonly used fractional order controllers. To guarantee fair comparisons, the controllers were designed according to the same phase margin ($\varphi_m = 60^\circ$). According to (7) and (8), the PMSM speed servo plant without the ESO-based compensation can be represented as

$$G(s) = \frac{60C_m/(2\pi J)}{s(L_q s/K_s + 1)} = \frac{187.57}{s(0.0039s + 1)}. \tag{38}$$

Firstly, the fractional order PI$^\lambda$D$^\mu$ controller was employed for a comparison. The PI$^\lambda$D$^\mu$ controller can be represented as

$$C(s) = K_p\left(1 + \frac{K_i}{s^\lambda} + K_d s^\mu\right), \tag{39}$$

where K_p, K_i and K_d are the proportional, integral and derivative gains, respectively; and λ and μ are the integral and derivative orders, respectively.

By applying a state transition algorithm (STA)-based tuning method [38], an PI$^\lambda$D$^\mu$ controller was designed with the ITAE index adopted as the objective function:

$$C_3(s) = 0.373\left(1 + \frac{27.867}{s^{0.945}} + 0.0021s^{1.085}\right). \tag{40}$$

Secondly, the fractional order controller based on the internal model control (IMC) strategy was also employed for comparison. Using a classic tuning method [39], an IMC controller was designed as follows.

$$Q_{\mathrm{IMC}}(s) = \frac{s(Ts + 1)}{K(1 + \tau s^\xi)}, \tag{41}$$

where $K = 60C_m/(2\pi J)$, $T = L_q/K_s$, τ and ξ are the controller parameters configuring the frequency characteristic of the servo system. Therefore, the equivalent feedback controller contained a PD controller and a fractional order integrator:

$$C_4(s) = \frac{Q_{\mathrm{IMC}}(s)}{1 - Q_{\mathrm{IMC}}(s)G(s)} = \frac{1.538}{s^{0.333}}(1 + 0.0039s). \tag{42}$$

Thirdly, as a commonly used, robust fractional order controller, the second generation CRONE controller was used. According to the CRONE design strategy [40], given the

design specifications ω_c and φ_m, the control system should have nearly the same phase characteristic as a fractional order integrator around the gain crossover frequency ω_c.

$$\beta(s) = \left(\frac{\omega_c}{s}\right)^{\nu}, \tag{43}$$

where ν is a fractional order determined by the phase margin φ_m. In addition, the integral part and low-pass part are introduced into the open-loop transfer function (43) to ensure the rejection of steady-state error and noise [40]. Therefore, according to the plant model (38) and the design specifications, the feedback controller was designed as

$$\begin{aligned} C_5(s) &= \frac{2\pi J {\omega_c}^{\nu}}{60 C_m}\left(1+\frac{\omega_l}{s}\right)\left[\frac{1}{s^{\nu-1}}\left(1+\frac{L_q}{K_s}s\right)\right]\frac{1}{1+s/\omega_h}, \\ &= 0.87\left(1+\frac{5}{s}\right)\left[\frac{1}{s^{0.199}}(1+0.0039s)\right]\frac{1}{1+s/500}. \end{aligned} \tag{44}$$

Step response experiments were implemented, applying the PI$^{\lambda}$D$^{\mu}$ controller $C_3(s)$ (denoted as FOPID), the IMC-based controller $C_4(s)$ (denoted as IMC-PID), the CRONE controller $C_5(s)$ (denoted as CRONE) and the proposed controller $C_1(s)$ with the ESO (FOPD-ESO) as the speed controller. The motor speeds and q-axis currents of the systems using FOPID, IMC-PID, CRONE and FOPD-ESO are plotted in Figure 9. In addition, the quantitative performance comparisons are presented in Table 5. It can be observed that FOPD-ESO provided the best step response performance.

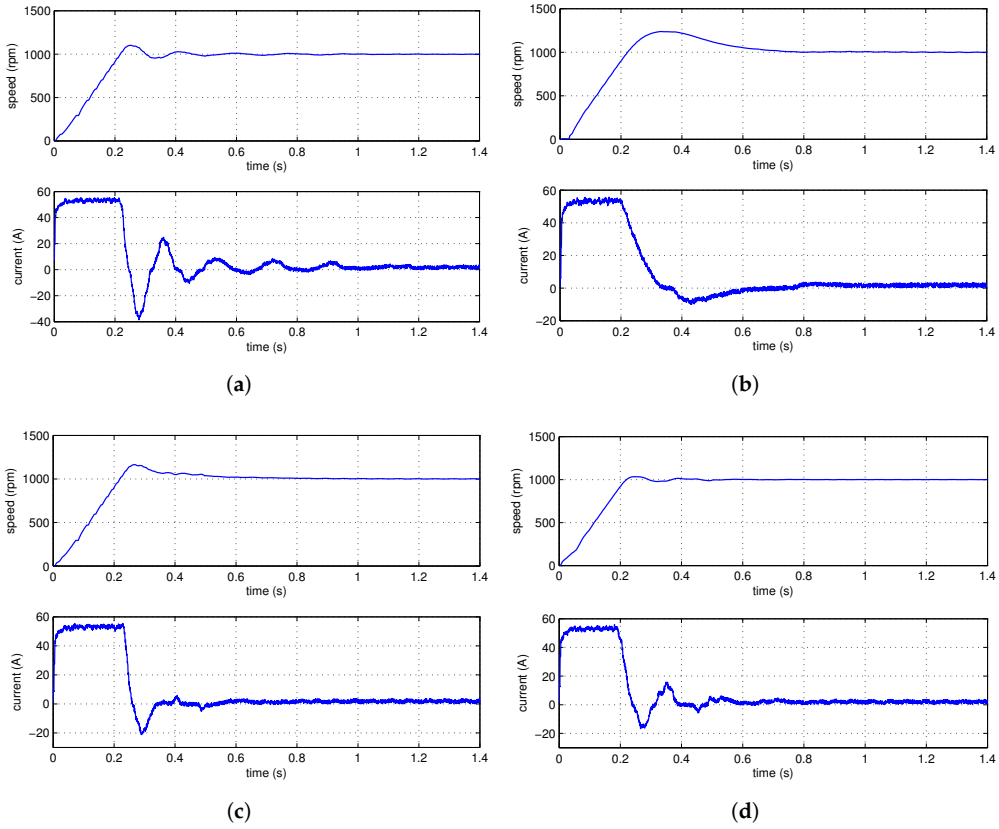

Figure 9. Step response comparisons. (**a**) FOPID. (**b**) IMC-PID. (**c**) CRONE. (**d**) FOPD-ESO.

Table 5. Step response performance indices of the systems.

Index	FOPID-STA	IMC-PID	CRONE	FOPD-ESO
Settling time (s)	0.243	0.605	0.452	0.207
Overshoot (%)	12.43	23.77	16.40	3.41

Load disturbance response experiments were also implemented. The partial enlarged curves of the motor speed and q-axis current of the systems using FOPID, IMC-PID, CRONE and FOPD-ESO are plotted in Figure 10. In addition, the quantitative performance comparisons are presented in Table 6. It can be observed that FOPD-ESO provided similar disturbance rejection performance to FOPID, and better performance than IMC-PID and CRONE.

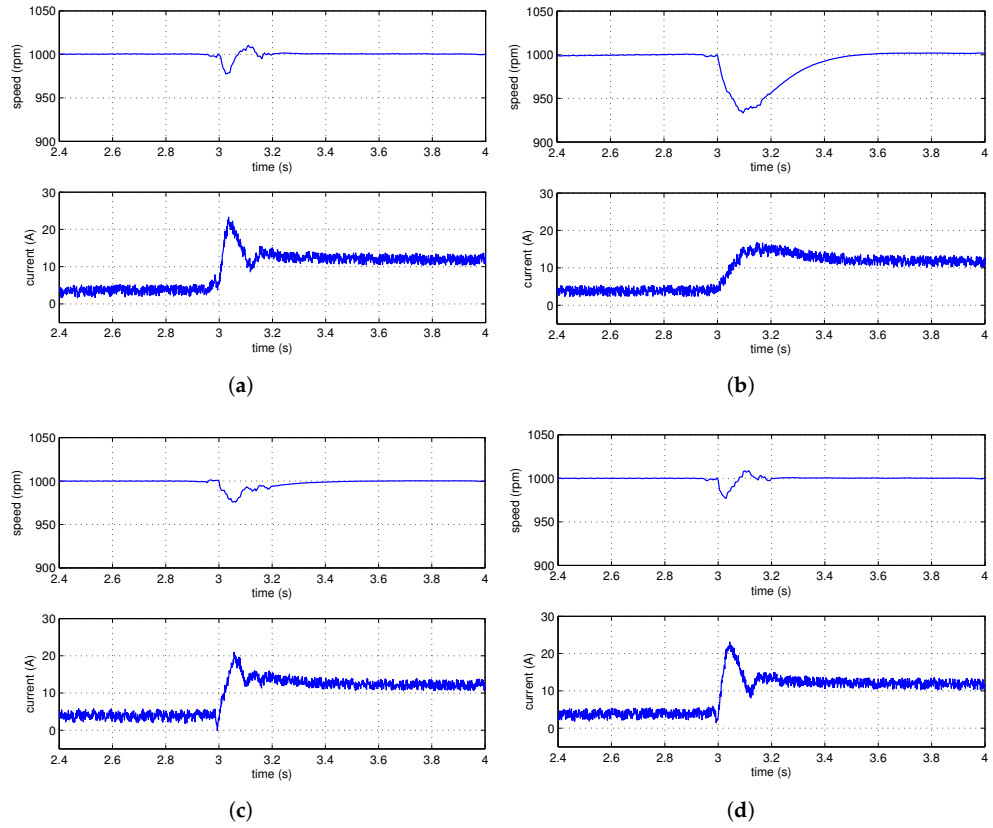

Figure 10. Load disturbance response comparisons. (**a**) FOPID. (**b**) IMC-PID. (**c**) CRONE. (**d**) FOPD-ESO.

Table 6. Load disturbance response performance indices of the systems.

Index	FOPID	IMC-PID	CRONE	FOPD-ESO
Dynamic speed drop (%)	2.26	6.65	2.42	2.30
Recovery time (s)	0.108	0.372	0.143	0.052

According to the experimental results, the FOPD-ESO control scheme can provide the optimal step response performance for the PMSM speed servo system and sufficient rejection to the load disturbances. Moreover, the FOPD-ESO controller had better overall control performance than the existing FOPID, IMC-PID and CRONE controllers.

5. Conclusions

A fractional order composite control scheme for the PMSM speed servo system was proposed. A ESO-based feedforward compensation scheme was proposed to improve the

robustness and convert the PMSM speed servo plant into a double-integrator model. In addition, a fractional order PD^{μ} controller was adopted to provide the optimal step response performance. A look-up table based synthesis method was proposed to simplify the tuning of the PD^{μ} controller and make it suitable for actual applications. The dynamic performance and robustness of the composite control system were demonstrated by simulations and experiments. For other classes of plants, a similar look-up table can be established according to specific design specifications. The success of the composite control scheme may be duplicated. For future work, some open issues to be studied include the control and synthesis strategies to cope with other types of uncertainties and disturbances; the further investigation of the controllability and optimal control schemes of fractional order systems; and the engineering applications of the proposed method.

Author Contributions: Conceptualization, Y.C. (YangQuan Chen); Methodology, W.Z. and R.H.; Investigation, W.Z. and Y.L.; resources, X.W.; writing, W.Z.; supervision, Y.C. (Yong Chen); funding acquisition, W.Z.; All authors have read and agreed to the published version of the manuscript.

Funding: This research was funded by the Natural Science Foundation of Guangdong, China grant number 2019A1515110180, the National Natural Science Foundation of China grant number 62173150 and 51975234, the Guangdong Province Science and Technology Planning Project grant number 2017A010102018, and the Projects of Guangdong Provincial Department of Education grant number 2017KQNCX215. The APC was funded by 2019A1515110180.

Data Availability Statement: The data presented in this study are available on request from the corresponding author.

Conflicts of Interest: The authors declare no conflict of interest.

References

1. Wakitani, S.; Yamamoto, T.; Gopaluni, B. Design and application of a database-driven PID controller with data-driven updating algorithm. *Ind. Eng. Chem. Res.* **2019**, *58*, 11419–11429. [CrossRef]
2. Yang, J.; Chen, W.; Li, S.; Guo, L.; Yan, Y. Disturbance/uncertainty estimation and attenuation techniques in PMSM drives—A survey. *IEEE Trans. Ind. Electron.* **2017**, *64*, 3273–3285. [CrossRef]
3. Yan, Y.; Yang, J.; Sun, Z.; Li, S.; Yu, X. Non-linear-disturbance-observer-enhanced MPC for motion control systems with multiple disturbances. *IET Control Theory A* **2020**, *14*, 63–72. [CrossRef]
4. Li, S.; Liu, Z. Adaptive speed control for permanent-magnet synchronous motor system with variations of load inertia. *IEEE Trans. Ind. Electron.* **2009**, *56*, 3050–3059.
5. Chen, D.; Guo, T.; Yang, J.; Li, S. A disturbance observer-based current-constrained controller for speed regulation of PMSM systems subject to unmatched disturbances. *IEEE Trans. Ind. Electron.* **2021**, *68*, 767–775.
6. Yuan, Y.; Wang, Z.; Yang, Y.; Guo, L.; Yang, H. Active disturbance rejection control for a pneumatic motion platform subject to actuator saturation: An extended state observer approach. *Automatica* **2019**, *107*, 353–361. [CrossRef]
7. Ran, M.; Wang, Q.; Dong, C.; Xie, L. Active disturbance rejection control for uncertain time-delay nonlinear systems. *Automatica* **2020**, *112*, 108692. [CrossRef]
8. Haji, V.H.; Monje, C.A. Fractional order fuzzy-PID control of a combined cycle power plant using particle swarm optimization algorithm with an improved dynamic parameters selection. *Appl. Soft Comput.* **2017**, *58*, 256–264. [CrossRef]
9. Shi, L.; Yuan, Y.; Gao, J.; Zhou, L.; Mao, J. Compact fractional-order model of on-chip inductors with BCB on high resistivity silicon. *IEEE Trans. Compon. Packag. Manuf. Technol.* **2020**, *10*, 878–886. [CrossRef]
10. Zheng, W.; Luo, Y.; Chen, Y.; Wang, X. Synthesis of fractional order robust controller based on Bode's ideas. *ISA Trans.* **2021**, *111*, 290–301. [CrossRef] [PubMed]
11. Shukla, A.; Patel, R. Controllability results for fractional semilinear delay control Systems. *J. Appl. Math. Comput.* **2021**, *65*, 861–875. [CrossRef]
12. Kavitha, K.; Vijayakumar, V.; Udhayakumar, R.; Sakthivel, N.; Nisar, K.S. A note on approximate controllability of the Hilfer fractional neutral differential inclusions with infinite delay. *Math. Methods Appl. Sci.* **2021**, *44*, 4428–4447. [CrossRef]
13. Vijayakumar, V.; Udhayakumar, R. A new exploration on existence of Sobolev-type Hilfer fractional neutral integro-differential equations with infinite delay. *Numer. Methods Partial Differ. Equ.* **2021**, *37*, 750–766. [CrossRef]
14. Raja, M.M.; Vijayakumar, V.; Udhayakumar, R. A new approach on approximate controllability of fractional evolution inclusions of order $1 < r < 2$ with infinite delay, Chaos. *Solitons Fractals* **2020**, *141*, 110343.
15. Ren, H.; Fan, J.; Kaynak, O. Optimal design of a fractional-order proportional-integer-differential controller for a pneumatic position servo system. *IEEE Trans. Ind. Electron.* **2019**, *66*, 6220–6229. [CrossRef]

16. Lin, X.; Liu, J.; Liu, F.; Liu, Z.; Gao, Y.; Sun, G. Fractional-order sliding mode approach of buck converters with mismatched disturbances. *IEEE Trans. Circuits Syst. I Regul. Pap.* **2021**, *68*, 3890–3900. [CrossRef]
17. Zheng, W.; Luo, Y.; Chen, Y.; Wang, X. A simplified fractional order PID controller's optimal tuning: a case study on a PMSM speed servo. *Entropy* **2021**, *23*, 130. [CrossRef] [PubMed]
18. Shah, P.; Agashe, S. Review of fractional PID controller. *Mechatronics* **2016**, *38*, 29–41. [CrossRef]
19. Sheng, Y.; Bai, W.; Xie, Y. Fractional-order $PI^{\lambda}D$ sliding mode control for hypersonic vehicles with neural network disturbance compensator. *Nonlinear Dyn.* **2021**, *103*, 849–863. [CrossRef]
20. Shi, X.; Chen, Y.; Huang, J. Application of fractional-order active disturbance rejection controller on linear motion system. *Control Eng. Pract.* **2018**, *81*, 207–214. [CrossRef]
21. Liu, L.; Zhang, S.; Chen, Y.; Xue, D. General robustness analysis and robust fractional-order PD controller design for fractional-order plants. *IET Control Theory A* **2018**, *12*, 1730–1736. [CrossRef]
22. Dastjerdi, A.; Saikumar, N.; HosseinNia, S. Tuning guidelines for fractional order PID controllers: Rules of thumb. *Mechatronics* **2018**, *56*, 26. [CrossRef]
23. Malek, H.; Luo, Y.; Chen, Y. Identification and tuning fractional order proportional integral controllers for time delayed systems with a fractional pole. *Mechatronics* **2013**, *23*, 746–754. [CrossRef]
24. Zheng, W.; Luo, Y.; Wang, X.; Pi, Y.; Chen, Y. Fractional order $PI^{\lambda}D^{\mu}$ controller design for satisfying time and frequency domain specifications simultaneously. *ISA Trans.* **2017**, *84*, 212–222. [CrossRef]
25. Deng, W.; Liu, H.; Xu, J.; Zhao, H.; Song, Y. An Improved Quantum-Inspired Differential Evolution Algorithm for Deep Belief Network. *IEEE Trans. Instrum. Meas.* **2020**, *69*, 7319-7327. [CrossRef]
26. Ruan, Y.; Yang, Y.; Chen, B. *Control System of Electric Drives–Motion Control Systems (In Chinese)*, 5th ed.; China Machine Press: Beijing, China, 2016.
27. Tursini, M.; Parasiliti, F.; Zhang, D. Decentralized tracking for a class of interconnected nonlinear systems using variable structure control. *IEEE Trans. Ind. Appl.* **2002**, *38*, 1018–1026. [CrossRef]
28. Lai, C.; Shyu, K. A novel motor drive design for incremental motion system via sliding-mode control method. *IEEE Trans. Ind. Electron.* **2005**, *52*, 499–507. [CrossRef]
29. Gao, Z. Scaling and bandwidth-parameterization based controller tuning. In Proceedings of the 2003 American Control Conference, Denver, CO, USA, 4–6 June 2003; Volume 6, pp. 4989–4996.
30. Chen, C. Stability. In *Linear System Theory and Design*, 3rd ed.; Oxford University Press: New York, NY, USA, 1999; pp. 121–125.
31. Kirk, D.E. *Optimal Control Theory: An Introduction*; Dover Publications: New York, NY, USA, 2004; pp. 1–3.
32. Asgharnia, A.; Shahnazi, R.; Jamali, A. Performance and robustness of optimal fractional fuzzy PID controllers for pitch control of a wind turbine using chaotic optimization algorithms. *ISA Trans.* **2018**, *79*, 27–44. [CrossRef] [PubMed]
33. Das, S.; Mullick, S.; Suganthan, P. Recent advances in differential evolution—An updated survey. *Swarm Evol. Comput.* **2016**, *27*, 1–3. [CrossRef]
34. Franklin, G.; Powell, J.; Emami-Naeini, A. *Feedback Control of Dynamic Systems*, 7th ed.; Pearson Education: London, UK, 2015.
35. Press, W.; Flannery, B.; Teukolsky, S.; Vetterling, W. *Numerical Recipes in C: The Art of Scientific Computing*, 2nd ed.; Cambridge University Press: Cambridge, UK, 1993.
36. Chen, Y. Impulse Response Invariant Discretization of Fractional Order Integrators/Differentiators, Filter Design and Analysis, MATLAB Central. Available online: http://www.mathworks.com/matlabcentral/fileexchange/21342-impulse-response-invariant-discretization-of-fractional-order-integrators-differentiators (accessed on 16 December 2021).
37. Ahn, H.; Chen, Y. Necessary and sufficient stability condition of fractional-order interval linear systems. *Automatica* **2008**, *44*, 2985–2988. [CrossRef]
38. Zhang, F.; Yang, C.; Zhou, X.; Gui, W. Fractional-order PID controller tuning using continuous state transition algorithm. *Neural Comput. Applic.* **2018**, *29*, 795–804. [CrossRef]
39. Bettayeb, M.; Mansouri, R. Fractional IMC-PID-filter controllers design for non integer order systems. *J. Process Control* **2014**, *24*, 261–271. [CrossRef]
40. Sabatier, J.; Lanusse, P.; Melchior, P.; Oustaloup, A. *Fractional Order Differentiation and Robust Control Design: CRONE, H-Infinity and Motion Control*; Springer: Dordrecht, The Netherlands, 2015.